Near ambient pressure XPS investigation of CO oxidation over $Pd_3Au(100)$

Marie D. Strømsheim[1], Jan Knudsen[2;3], Mari H. Farstad[1], Linn Sørvik[1], Xiaoyang Guo[1], Hilde J. Venvik[1*], and Anne Borg[4,]

[1]Department of Chemical Engineering, NTNU - Norwegian University of Science and Technology, NO-7491 Trondheim, Norway

[2]MAX IV Laboratory, Lund University, Box 118, SE-221 00 Lund, Sweden,

[3]Division of Synchrotron Radiation Research, Lund Univ.,Box 118, SE-221 00 Lund, Sweden

[4]Department of Physics, NTNU - Norwegian University of Science and Technology, NO-7491 Trondheim, Norway

* Corresponding Author: hilde.j.venvik@ntnu.no

Keywords: CO oxidation, near ambient x-ray photoelectron spectroscopy, quadrupole mass spectrometry, $Pd_3Au(100)$, hysteresis

ABSTRACT

The CO oxidation behavior under excess oxygen and near stoichiometric conditions over the surface of $Pd_3Au(100)$ has been studied by combining near-ambient pressure X-ray photoelectron spectroscopy and quadrupole mass spectrometry and compared to Pd(100). During heating and cooling cycles, normal hysteresis in the CO_2 production, i.e. with the light-off temperature being higher than the extinction temperature, is observed for both surfaces. On both $Pd_3Au(100)$ and Pd(100) the $(\sqrt{5}x\sqrt{5})R27°$ surface oxide structure is present during CO_2 production under excess oxygen conditions (O_2:CO = 10:1), while at near stoichiometric conditions (O_2:CO = 1:1) the surfaces are covered with atomic oxygen. Au as alloying element hence induces only minor differences in the observed hysteresis and the active phase compared to pure Pd. Alloying with Au thus yields a different behavior compared to Ag, where reversed hysteresis is observed for CO_2 production over $Pd_{75}Ag_{25}(100)$ at similar conditions [Fernandes et al., ACS Catal. (2016) 4154]

1. INTRODUCTION

Palladium is a preferred catalyst for a number of reactions, including the oxidation of hydrocarbons [1,2] and CO [3,4], and the state of the active Pd surface during reaction has been extensively discussed [5,6]. Surface oxides rather than surfaces covered by chemisorbed oxygen have been observed as the most active towards CO oxidation under near ambient as well as more realistic conditions (above ambient pressure) [5–16]. However, some studies also indicate Pd surfaces covered by atomic oxygen as highly active [8,17], and generally both will exhibit activity. For Pd(100), the presence of a ($\sqrt{5}$x$\sqrt{5}$)R27° surface oxide (henceforth denoted $\sqrt{5}$) is found to exist when the surface is highly active towards CO oxidation [5,6,8,10,14,17,18], and this is consistent with the reaction following a Mars-van Krevelen mechanism with gas-phase CO reacting with the surface oxide to form CO_2 [5–7,9,11,13–15,19]. The presence of the surface oxide during high CO_2 production is also supported by kinetic Monte-Carlo simulations [20,21].

Bimetallic systems provide routes for improved catalyst performance through modification of selectivity and activity, demonstrated for example for catalytic oxidation [22] and reforming [23]. Typical alloying elements for Pd based catalysts include among others Cu [24–26], Ag [27] and Au [28]. Pd-Au alloys have been increasingly investigated in regards to low temperature CO oxidation [29–32], with the addition of Au reported to enhance the activity of the Pd-based catalysts [30].

Introducing a secondary element adds complexity in terms of reaction dynamics. Both for nanoparticles [32,33] and single crystal surfaces [19,29,34–36] it has been shown that adsorbates and reactions may induce segregation and restructuring. In the case of Au as alloying element with Pd, the lower surface energy of Au in absence of adsorbates yields a driving force for segregation of Au to the surface under ultra-high vacuum (UHV) conditions [37]. Differences in bond energy of chemisorbed species affect the segregation behavior [38,39]. Experimental studies on PdAu(100) [29,34], and PdAu(110) [36] have shown that exposure to CO pressures above 0.13 mbar and temperatures below and close to RT induces segregation of Pd, resulting in the formation of contiguous Pd sites at the surface [29,34]. Similarly, a higher amount of neighboring Pd atoms, important for O_2 dissociation has been found experimentally [29,40] and theoretically [41,42] as a

result of exposure to O_2. The formation of a √5 surface oxide on $Pd_{75}Ag_{25}$(100) [35], similar to the √5 oxide observed on Pd(100) [43], is also a result of chemisorption driven segregation. As opposed to Pd(100), the oxide on $Pd_{75}Ag_{25}$(100) consists of a pure Pd-oxide residing on top of a Ag rich layer that serves as an interface to the $Pd_{75}Ag_{25}$ bulk. Adsorbate-induced segregation in $Pd_{1-x}Ag_x$ is also predicted theoretically as a result of oxygen [33,44], hydrogen [44–47], and CO [44] adsorption.

In the present work, we focus on the effect of Au as an alloying element with Pd on the CO oxidation reaction, by comparing the Pd_3Au(100) model system to the corresponding pure Pd and $Pd_{75}Ag_{25}$ surfaces (note that whilst Pd forms an ordered alloy upon replacement of 25% of the atoms with Au, this is not the case with Ag, hence the different notations). Near ambient pressure X-ray photoelectron spectroscopy (NAPXPS) investigations coupled with concurrent quadrupole mass spectrometry (QMS) measurements have been performed to elucidate the state of the Pd_3Au(100) surface during reaction. In particular, the influence of the alloying element during temperature ramping will be discussed.

2. EXPERIMENTAL METHOD

Pd_3Au(100) and Pd(100) single crystals were cleaned by cycles of sputtering, and annealing at 500°C and 700 °C respectively, with and without oxygen. Temperatures were measured with a type K thermocouple spot-welded to the edge of the crystal. The cleanliness of the surfaces was checked by XPS measurement of the C 1s and S 2p core level spectra.

NAPXPS measurements were performed at the SPECIES [48,49] beam line of the MAX IV Laboratory. The beam line was equipped with a SPECS PHOIBOS 150 NAP analyzer for near ambient pressure measurements and a reaction cell, which is filled with gases during experiments. The NAPXPS data were recorded *in situ* at gas pressures about 1 mbar, and total gas flows of 1.0-2.0 cm^3/min were applied. A QMS connected to the gas exit lines via a leak valve was applied to monitor the gas composition at the outlet of the reaction cell. The QMS instrument was a Dycor LC-D Residual Gas Analyzer from AMTEK. The oxidation experiments were carried out by introducing O_2 and CO at a ratio of approximately 10:1 or 1:1, denoted excess oxygen and near stoichiometric conditions, respectively. The sample temperature was ramped from room temperature (RT) to 325°C

and back in several cycles. Simultaneous NAPXPS, QMS, and temperature data were collected during the experiments. Previously reported CO oxidation experiments over Pd(100) at ratio 10:1 performed at beamline I511 at MAX IV Laboratory [50] have also been included here, with the experimental details described in ref. [19].

The core level spectra of the O 1s, Pd 3d, Au 4f and C 1s region were measured at photon energies of 650, 400, 220 eV and 400 eV, respectively. The Pd $3d_{3/2}$ core level was also analyzed in order to determine possible contributions from Au $4d_{5/2}$ (binding energy 335.0 eV). The cross sections of Au 4d and Pd 3d are 0.4 and 3.5, respectively, at 400 eV photon energy [51]. No significant contribution from Au 4d to the intensity was found upon comparing the Pd $3d_{3/2}$ and the Pd $3d_{5/2}$ spectra. Hence Pd $3d_{5/2}$ is presented in the current work. All spectra were measured at normal emission. The binding energy was calibrated by recording the Fermi edge immediately after the core level regions. Linear background was applied and Doniach-Sunjic line shapes used for fitting the spectra [52]. Normalization was carried out with respect to the background on the low binding energy side.

The LEED experiments were performed in our home UHV system, with base pressure below $1x10^{-10}$ mbar. The $Pd_3Au(100)$ surface was oxidized at a temperature of ~300 °C and an oxygen pressure of approximately 10^{-3} mbar, obtained by placing a microchannel plate oxygen doser close to the sample surface.

3. RESULTS AND DISCUSSION

The √5 surface oxide structure on Pd(100) is well documented [43,53] and is, as stated above, known to be the active phase during CO oxidation in excess oxygen [19] at near ambient conditions. An image of the LEED pattern for this oxide structure obtained by exposing the single crystal surface to O_2 at about 10^{-5} mbar and ~ 320 °C is shown in Figure 1 (bottom). Also on $Pd_{75}Ag_{25}(100)$, a similar √5 oxide is formed, but somewhat higher oxygen pressure is required [35]. For the sake of discussion of the CO oxidation over $Pd_3Au(100)$ we have investigated if a √5 surface oxide structure can also be formed on this alloy surface. Figure 1 (top) shows the LEED pattern obtained after oxygen exposure of $Pd_3Au(100)$ at about 10^{-3} mbar and ~300 °C, i.e. similar conditions as applied for $Pd_{75}Ag_{25}(100)$.

The presence of a √5 surface oxide structure also on $Pd_3Au(100)$ is hence confirmed but the pattern is less sharp compared to that recorded for Pd(100). This was also the case for $Pd_{75}Ag_{25}(100)$ [35] and attributed to smaller √5 domains as well as possible presence of atomic oxygen species. The observed √5 surface oxide formation on $Pd_3Au(100)$ is in line with the trend that adsorption of species with a strong interaction with Pd, generally makes segregation of Pd to the surface energetically favorable for Pd-alloys where the alloying element has a weaker interaction with the adsorbed species, e.g Ag [33,44].

The NAPXPS Pd $3d_{5/2}$ spectra for the active Pd(100) and $Pd_3Au(100)$ surfaces for CO_2 production under excess oxygen conditions and elevated temperature are presented in Figure 2. The previously analyzed spectrum for Pd(100) [19] is first discussed as a basis for the interpretation for $Pd_3Au(100)$. The Pd $3d_{5/2}$ spectrum recorded at ~230°C for Pd(100) under exposure to O_2:CO at ratio 10:1, and total pressure ~0.7 mbar, is presented in the lower panel of Figure 2. Beside the bulk Pd binding energy (BE) at 334.8 eV, the spectrum includes peaks attributed to Pd 2-fold and 4-fold coordinated with oxygen (henceforth denoted 2-fold and 4-fold peaks) at 335.3 eV and 336.1 eV, respectively. These represent a fingerprint of the √5 surface oxide [43]. In addition, there is an interface component at 334.7 eV that is attributed to Pd atoms in the layer directly underneath the surface oxide [43]. The spectral weights of the 2-fold and 4-fold contributions are similar, indicating a surface with comparable amounts of the two oxygen-coordinated species.

Turning to the $Pd_3Au(100)$ surface, the upper panel of Figure 2 displays the NAPXPS Pd $3d_{5/2}$ core level spectrum obtained at ~325°C upon exposure of O_2 and CO at ratio 10:1 and total pressure ~1 mbar. In addition to the bulk contribution at 334.6 eV, two √5 oxide components at binding energies 335.2 eV and 336.0 eV can be identified. Compared to Pd(100) there are some differences in peak positions. The bulk Pd peak is shifted by 0.3 eV towards lower BE for Pd_3Au. This shift can be attributed to the presence of Au as alloying element. A similar shift relative to the pure Pd bulk is also observed for $Pd_{75}Ag_{25}(100)$ [35]. The Au $4f_{7/2}$ core level (not shown) is also shifted towards lower BE by ~0.6 eV for Pd_3Au relative to pure Au. A discussion of the core level shifts in the PdAu-alloy is beyond the scope of the present work, but has been previously been

addressed by Olovsson et al. [54]. Since the surface oxide incorporates Pd atoms only, the √5 oxide peak positions are similar for Pd(100), $Pd_3Au(100)$ and $Pd_{75}Ag_{25}(100)$. Nevertheless, the 4-fold oxide peak for the two alloys is shifted by ~0.1 eV towards lower binding energy relative to the 4-fold peak for Pd(100) [19,35]. As mentioned, a Pd $3d_{5/2}$ interface component was assigned for the √5 surface oxide on Pd(100) [19,43]. In contrast, UHV studies of the √5 oxide on $Pd_{75}Ag_{25}(100)$ revealed that the layer beneath the oxide consists of a high amount of Ag [35]. The current spectra cannot discern whether an interface component is present for the √5 surface oxide on $Pd_3Au(100)$ or not. This is partly due to limited spectral resolution at elevated temperatures. In addition, the close proximity in peak position of the bulk Pd and the interface peak in the Pd $3d_{5/2}$ spectrum of $Pd_3Au(100)$ makes these two contributions difficult to deconvolute. The presence of the √5 surface oxide on $Pd_3Au(100)$ is in clear contrast to the behavior of $Pd_{75}Ag_{25}(100)$, for which the Pd $3d_{5/2}$ core level spectrum displayed no signature of the √5 surface oxide, and only chemisorbed oxygen was present on the surface under equivalent conditions [41].

There are certain differences between the Pd $3d_{5/2}$ core level spectra of the √5 oxides investigated on the different (100) terminated Pd based surfaces. For $Pd_3Au(100)$, the spectral weight of the 2-fold peak is significantly larger than that of the 4-fold peak, while the two oxide contributions observed for Pd(100) are relatively similar [43]. The presence of Au has been reported to result in Pd being more difficult to oxidize for supported Pd-Au catalysts during CO oxidation [28]. Gao et al.[34] observed that exposing PdAu(100) to a mixture of O_2:CO = 8:1 at 277°C did not result in oxidation of the surface, while this was the case for Pd(100). Investigations by XPS and XANES of polycrystalline Pd-Au alloys furthermore determined that there is a small net charge transfer from Pd to Au upon alloying [55]. Finally, a higher spectral weight of the 2-fold peak in comparison to the 4-fold peak was also reported for $Pd_{75}Ag_{25}(100)$ by Walle et al.[35] that, together with the aforementioned lower degree of long range order observed in LEED, was suggested to originate from the presence of chemisorbed oxygen. The difference in relative intensity between the oxide contributions and the smaller degree of long range order inferred from LEED hence support the interpretation that the surface oxide is not entirely covering the $Pd_3Au(100)$ surface. The lower surface oxide coverage of

$Pd_3Au(100)$ relative to pure Pd could also contribute towards differences in the relative intensities of the bulk Pd peaks in the Pd $3d_{5/2}$ spectra of the $\sqrt{5}$ oxide.

The surface of Pd(100) is covered with adsorbed CO at low temperature under exposure to O_2 and CO in excess oxygen (10:1), as shown in the previously reported Pd $3d_{5/2}$ spectrum obtained at 80°C and displayed in the lower panel of Fig. 3 [19]. The only peak besides bulk Pd is found at BE 335.5 eV and originates from adsorbed CO. The corresponding Pd $3d_{5/2}$ core level spectrum for $Pd_3Au(100)$, obtained at RT and oxygen rich CO oxidation conditions (Figure 3, upper panel), also contains two contributions. Equivalent to Pd(100), one can be assigned to bulk Pd at 334.6 eV BE and the other to adsorbed CO at 335.4 eV. Noteworthy, the spectral weight of the CO induced component for $Pd_3Au(100)$ is similar to that of Pd(100). Since CO normally interacts weakly with Au, the similar spectral weight suggests that the surface is composed mainly of Pd. However, CO is also reported to adsorb on PdO(101) at low temperature, with a O 1s contribution from surface oxygen atoms remaining after CO exposure [56]. Such a contribution cannot be resolved from the CO induced contribution in the Pd $3d_{5/2}$ spectrum, but may be discerned from the corresponding O 1s spectra as will be discussed below.

The oxidation of CO in excess O_2 over $Pd_3Au(100)$ was monitored as a function of sample temperature by performing NAPXPS measurements recording the Pd $3d_{5/2}$ core level region together with QMS data, while heating the sample temperature from about RT to selected, high temperatures and cooling down again towards RT. Similar series recording the O1s core level region were also performed.

Figure 4a displays recording of the O 1s region spectral series during heating to 325°C followed by cooling to RT in excess O_2, together with the corresponding QMS data. Details of the O1s region at representative high and low temperatures are also included (Figure 4b). At low temperature, the CO_2 QMS signal originates only from the residual gas in the reaction cell. The CO_2 signal starts to increase at about 160°C and reaches a maximum at about 195°C. Further increase in the temperature does not affect the CO_2 signal, implying that the reaction becomes mass-transfer limited at this point, as previously also reported for Pd(100)[6]. Upon reducing the temperature, the

CO_2 production is maintained until about 160°C where the production rapidly decreases and eventually extinguishes.

Figure 4b shows the $Pd_3Au(100)$ O 1s core level spectrum acquired before starting the temperature increase (bottom), and at 325 °C (top). At room temperature, the spectrum displays gas phase oxygen peaks located at 538.3 eV, and 537.4 eV, and a peak at 531.2 eV attributed to adsorbed CO. This is again analogous to Pd(100) and a surface covered by CO [19]. The spectral contribution from gas phase CO is not resolved at these conditions. The spectrum also includes a broad contribution from the Pd $3p_{3/2}$ core level centered at 531.8 eV. From the C 1s spectrum acquired at RT (Figure 4c) the CO is determined to be adsorbed in a Pd-Pd bridge position (~285.7 eV), based on the binding energy being similar as reported for CO adsorbed in bridge positions on pure Pd(100) [57]. There is a small shoulder at the high binding energy side of this peak (~286.8 eV), which might be attributed to CO adsorbed on top of isolated Pd atoms, as was done for $Pd_{70}Au_{30}(111)$ by Toyoshima et al. [58], and from considering the general trend for the C1s binding energy of CO adsorbed on Pt-group metal surfaces increasing with lower coordination with the metal surface [59,60]. The C 1s spectrum also includes a small CO gas phase contribution at BE ~290.0 eV.

The O 1s spectrum furthermore includes a component at ~529.6 eV, not observed on pure Pd(100) under comparable conditions [19], which may be assigned to adsorbed oxygen. Dissociation of O_2 on contiguous Pd sites on PdAu(100) has been reported by Gao et al. [29,34]. It was conjectured that dissociated O_2 from these sites would spill over to Au and isolated Pd sites, allowing CO oxidation to occur on these sites, as well as on contiguous Pd. Theoretical studies supporting these experimental findings have shown that sites consisting of at least four Pd atoms prefer to bind O_2 rather than CO, resulting in dissociation of O_2 [41]. These reports together with the aforementioned findings of van den Bossche et al.[56] support the interpretation that the origin of the additional component at low binding energy in the O1s spectrum is due to adsorbed oxygen.

Upon increasing the temperature, a shift of 0.1-0.2 eV towards higher binding energy in the O 1s contribution from gas phase O_2 is observed. This shift coincides with the surface becoming highly active towards CO_2 production and is caused by a change in the surface work function. The shift is accompanied by the appearance of additional peaks in the spectra and disappearance of the adsorbed

CO contribution. The O 1s spectrum recorded at 325°C hence contains a small component from CO_2 in the gas phase at ~535.1 eV binding energy, as well as the fingerprint peaks of the √5 located at 528.8 eV and 529.6 eV [43]. Comparatively, the shift in the O_2 gas phase peaks reported for Pd(100) is ~0.5 eV to higher binding energy [19], which is considerably larger than for $Pd_3Au(100)$. The relatively small shift in the O_2 gas phase peaks upon transitioning from a CO covered surface to the active surface towards CO_2 production indicates a smaller change in the work function and hence the surface chemistry for $Pd_3Au(100)$. The presence of atomic oxygen at both low and high temperature may explain this.

The active surface towards CO_2 production under excess oxygen is thus similar for the (100) termination of Pd_3Au and Pd, with both surfaces being partially or fully covered by a √5 surface oxide. At near stoichiometric conditions (O_2:CO = 1:1) and 0.7-1 mbar total pressures, however, the surface of Pd(100) is reported as covered by adsorbed oxygen during high CO_2 production [6]. In order to obtain a more complete comparison of the Pd(100) and $Pd_3Au(100)$ surfaces, the reaction was performed in O_2 and CO at 1:1 for $Pd_3Au(100)$. The O 1s and C 1s core level spectra are presented in Figure 5 for low temperature. At RT, the peak assigned to adsorbed oxygen is still present (left panel) and in addition there is a peak originating from gas phase CO at BE 536.3 eV. The C 1s core level spectrum (right panel) indicates that CO is adsorbed in bridge position on Pd, as was found for 10:1. Figure 6 shows the O 1s and Pd $3d_{5/2}$ in the region of high catalytic activity at 325 °C under 1:1 conditions. No contribution due to Pd atoms 4-fold coordinated to oxygen can be observed in the $Pd3d_{5/2}$ spectrum (right panel), only contributions at 335.2 eV and bulk Pd at 334.7 eV consistent with a surface with chemisorbed oxygen atoms. The corresponding O 1s spectrum (left panel) shows a high relative concentration of CO_2 in the gas phase, the contribution located at 535.4 eV binding energy, and a single peak at 529.2 eV assigned to chemisorbed oxygen. The Pd $3d_{5/2}$ core level spectrum acquired at near stoichiometric O_2:CO ratio (Figure 6, right panel) is hence consistent with a surface covered with chemisorbed oxygen, with no trace of the fingerprint signature of the √5 oxide observed. Again the behavior is similar to that of Pd(100) [6,19].

The light-off-extinction behavior during reaction can be analyzed by plotting the CO_2 QMS data versus temperature. Such hysteresis curves have previously been reported for the CO oxidation

reaction under excess oxygen conditions for Pd(100) and $Pd_{75}Ag_{25}$(100) [19]. The hysteresis curve for the Pd_3Au(100) surface under corresponding conditions is displayed in Figure 7a, showing the light-off occurring at 195 °C and the extinction of the reaction at about 160°C. This gives a bistability window of approximately 40 °C, and a normal hysteresis attributable to the effect of coverage [61]. The light-off and extinction corresponds to the observed change in surface chemistry in Figure 4a, where the surface transitions from predominantly CO covered to a √5 oxide, and back. This is comparable to the behavior previously observed on Pd(100) [19], with the reported lift-off and extinction occurring at about 195 °C and 150 °C, giving similar bistability windows for the two surfaces. In the Ag case the behavior is quite different. The experimental light-off was observed to be at 200 °C, whereas the extinction was at 225 °C, representing inversed hysteresis. Furthermore, the reaction was not mass transfer limited. The reversed hysteresis was explained by an Ag-enrichment of the surface layer during temperature increase, with the high Ag concentration remaining during temperature decrease. The interpretation was supported by NAPXPS measurements of the combined Pd 3d and Ag 3d core regions which showed a higher Ag/Pd ratio following a temperature cycle [19]. In comparison, the current NAPXPS measurements of the combined Pd 3d and Au 4f region for Pd_3Au(100) before and after a temperature cycle did not show a significant change in the ratio between Au and Pd.

The QMS data recorded during the temperature cycle with near stoichiometric ratio are shown in Figure 7b for both Pd(100) (top) and Pd_3Au(100). The bistability window is shifted to higher temperature for both surfaces relative to the case of large excess of oxygen. The curves agree with previous investigations on Pd(100) establishing that the CO oxidation reaction is mass-transfer limited under near stoichiometric conditions, with the active surface being metallic Pd(100) with adsorbed oxygen [6]. Similarly as above, there is no significant change in Au/Pd ratio upon cycling. The light-off temperature occurs at 255 °C for Pd(100) and 265 °C for Pd_3Au(100), with the corresponding extinction temperatures at ~190 °C and 215 °C. The increased temperatures for light-off and extinction at near stoichiometric conditions may be attributed to a more persistent CO inhibition, and corresponding lower O_2 activation due to the increased CO and decreased O_2 partial pressure relative to the excess oxygen case. Regarding the difference in light-off temperature between Pd(100) and

$Pd_3Au(100)$, it is too early to conclude on the magnitude and origin. It is important to note that there are small differences in the bistability window range of 10-15°C between temperature cycles, which may be attributed to differences in the heating rate. Nevertheless, the difference is largest upon extinction, for which the transition occurs at ~25°C higher temperature over $Pd_3Au(100)$, which may be attributed to lower stability of the surface oxide with Au atoms present in the surface. Conclusions on Au induced differences in light-off temperatures require further experimental investigations as well as modeling.

4. CONCLUSION

The CO oxidation behavior over the surface of $Pd_3Au(100)$ has been investigated combining near-ambient pressure X-ray photoelectron spectroscopy and quadrupole mass spectrometry, and compared to similar experiments performed over Pd(100). As previously established for Pd(100), a $(\sqrt{5}x\sqrt{5})R27°$ surface oxide is found to exist on $Pd_3Au(100)$ during both CO_2 production at 10:1 ratio of O_2 and CO and after oxidation in UHV. But relative to pure Pd, the presence of Au seems to result in less long range order of the surface oxide and also parts of the surface covered by chemisorbed oxygen. Performing the reaction over $Pd_3Au(100)$ in O_2 and CO at 1:1 ratio furthermore yielded similar surface chemistry as for Pd(100), with atomic oxygen and not the $\sqrt{5}$ oxide being present on the surface during CO_2 production. During heating and cooling cycles, the observed light-off temperature for CO_2 production is always higher than the extinction temperature, i.e. normal hysteresis behavior attributable to CO coverage effects similar to that of Pd(100). In contrast, reversed hysteresis is observed for $Pd_{75}Ag_{25}(100)$ and only atomic oxygen is observed on the surface during the CO_2 production. Alloying Pd with Au thus yields a very different behavior compared to alloying with Ag, but relatively similar compared to pure Pd in terms of observed hysteresis and active phase.

ACKNOWLEDGMENT

Financial support has been received from from inGAP (Innovative Natural Gas Processes and Products), a centre for research based innovation appointed by the Research Council of Norway (Project No. 174893/O30), NordForsk (Grant No. 40521) Statoil ASA through the Gas Technology Centre (NTNU-SINTEF) and NTNU, and project grant 2012-3850 financed by the Swedish Research Council. We also thank the MAX IV Laboratory staff for excellent support. The contribution to initial discussions and data analysis by Dr. Vasco R. Fernandes are thankfully acknowledged.

REFERENCES

[1] P. Gélin, M. Primet, Appl. Catal. B Environ. 39 (2002) 1.

[2] D. Ciuparu, M.R. Lyubovsky, E. Altman, L.D. Pfefferle, A. Datye, Catal. Rev. 44 (2002) 593.

[3] J. Szanyi, D.W. Goodman, J. Phys. Chem. 98 (1994) 2972.

[4] R.M. Heck, R.J. Farrauto, Catalytic Air Pollution Control: Commercial Technology, 3rd ed., Van Nostrand Reinhold, 2009.

[5] B.L.M. Hendriksen, S.C. Bobaru, J.W.M. Frenken, Surf. Sci. 552 (2004) 229.

[6] S. Blomberg, M.J. Hoffmann, J. Gustafson, N.M. Martin, V.R. Fernandes, A. Borg, Z. Liu, R. Chang, S. Matera, K. Reuter, E. Lundgren, Phys. Rev. Lett. 110 (2013) 117601.

[7] A. Piednoir, M.A. Languille, L. Piccolo, A. Valcarcel, F.J. Cadete Santos. Aires, J.C. Bertolini, Catal. Letters 114 (2007) 110.

[8] M. Chen, X. V Wang, L. Zhang, Z. Tang, H. Wan, Langmuir 26 (2010) 18113.

[9] B.L.M. Hendriksen, M.D. Ackermann, R. van Rijn, D. Stoltz, I. Popa, O. Balmes, A. Resta, D. Wermeille, R. Felici, S. Ferrer, F.W. M., Nat Chem 2 (2010) 730.

[10] R. van Rijn, O. Balmes, R. Felici, J. Gustafson, D. Wermeille, R. Westerström, E. Lundgren, J.W.M. Frenken, J. Phys. Chem. C 114 (2010) 6875.

[11] R. van Rijn, O. Balmes, A. Resta, D. Wermeille, R. Westerström, J. Gustafson, R. Felici, E. Lundgren, J.W.M. Frenken, Phys. Chem. Chem. Phys. 13 (2011) 13167.

[12] A. Hellman, A. Resta, N.M. Martin, J. Gustafson, A. Trinchero, P.-A. Carlsson, O. Balmes, R. Felici, R. van Rijn, J.W.M. Frenken, J.N. Andersen, E. Lundgren, H. Grönbeck, J. Phys. Chem. Lett. 3 (2012) 678.

[13] R. Toyoshima, M. Yoshida, Y. Monya, Y. Kousa, K. Suzuki, H. Abe, B.S. Mun, K. Mase, K. Amemiya, H. Kondoh, J. Phys. Chem. C 116 (2012) 18691.

[14] R. Toyoshima, M. Yoshida, Y. Monya, K. Suzuki, B.S. Mun, K. Amemiya, K. Mase, H. Kondoh, J. Phys. Chem. Lett. 3 (2012) 3182.

[15] R. Toyoshima, M. Yoshida, Y. Monya, K. Suzuki, K. Amemiya, K. Mase, B.S. Mun, H. Kondoh, J. Phys. Chem. C 117 (2013) 20617.

[16] M. Shipilin, J. Gustafson, C. Zhang, L.R. Merte, A. Stierle, U. Hejral, U. Ruett, O. Gutowski, M. Skoglundh, P.-A. Carlsson, E. Lundgren, J. Phys. Chem. C 119 (2015) 15469.

[17] F. Gao, Y. Wang, Y. Cai, D.W. Goodman, J. Phys. Chem. C 113 (2009) 174.

[18] R. Westerström, M.E. Messing, S. Blomberg, A. Hellman, H. Grönbeck, J. Gustafson, N.M. Martin, O. Balmes, R. van Rijn, J.N. Andersen, K. Deppert, H. Bluhm, Z. Liu, M.E. Grass, M. Hävecker, E. Lundgren, Phys. Rev. B 83 (2011) 115440.

[19] V.R. Fernandes, M. Van den Bossche, J. Knudsen, M.H. Farstad, J. Gustafson, H.J. Venvik, H. Grönbeck, A. Borg, ACS Catal. (2016) 4154.

[20] J. Rogal, K. Reuter, M. Scheffler, Phys. Rev. Lett. 98 (2007) 46101.

[21] J. Rogal, K. Reuter, M. Scheffler, Phys. Rev. B 75 (2007) 205433.

[22] F. Tao, M.E. Grass, Y. Zhang, D.R. Butcher, J.R. Renzas, Z. Liu, J.Y. Chung, B.S. Mun, M. Salmeron, G.A. Somorjai, Science (80-.). 322 (2008) 932.

[23] M. Sankar, N. Dimitratos, P.J. Miedziak, P.P. Wells, C.J. Kiely, G.J. Hutchings, Chem. Soc. Rev 41 (2012) 8099.

[24] F. Wang, H. Zhang, D. He, Environ. Technol. 35 (2014) 347.

[25] K. Choi, M.A. Vannice, J. Catal. 131 (1991) 36.

[26] V. Sanchez-Escribano, L. Arrighi, P. Riani, R. Marazza, G. Busca, Langmuir 22 (2006) 9214.

[27] C. Norris, H.P. Myers, J. Phys. F Met. Phys. 1 (1971) 62.

[28] A.M. Venezia, L.F. Liotta, G. Pantaleo, V. La Parola, G. Deganello, A. Beck, Z. Koppány, K. Frey, D. Horváth, L. Guczi, Appl. Catal. A, Gen. 251 (2003) 359.

[29] F. Gao, Y. Wang, D.W. Goodman, J. Am. Chem. Soc. 131 (2009) 5734.

[30] J. Xu, T. White, P. Li, C. He, J. Yu, W. Yuan, Y.-F. Han, J. Am. Chem. Soc. 132 (2010) 10398.

[31] Z. Li, F. Gao, W.T. Tysoe, J. Phys. Chem. C 114 (2010) 16909.

[32] S. Alayoglu, F. Tao, V. Altoe, C. Specht, Z. Zhu, F. Aksoy, D.R. Butcher, R.J. Renzas, Z. Liu, G.A. Somorjai, Catal. Letters 141 (2011) 633.

[33] B.C. Khanra, M. Menon, Phys. B Condens. Matter 291 (2000) 368.

[34] F. Gao, Y. Wang, D.W. Goodman, J. Phys. Chem. C 113 (2009) 14993.

[35] L.E. Walle, H. Grönbeck, V.R. Fernandes, S. Blomberg, M.H. Farstad, K. Schulte, J. Gustafson, J.N. Andersen, E. Lundgren, A. Borg, Surf. Sci. 606 (2012) 1777.

[36] M.A. Languille, E. Ehret, H.C. Lee, C.K. Jeong, R. Toyoshima, H. Kondoh, K. Mase, Y. Jugnet, J.C. Bertolini, F.J.C.S. Aires, B.S. Mun, Catal. Today 260 (2016) 39.

[37] C.-W. Yi, K. Luo, T. Wei, D.W. Goodman, J. Phys. Chem. B 109 (2005) 18535.

[38] D. Tománek, S. Mukherjee, V. Kumar, K.H. Bennemann, Surf. Sci. 114 (1982) 11.

[39] L.C.A. van den Oetelaar, O.W. Nooij, S. Oerlemans, A.W. van der Gon, H.H. Brongersma, L. Lefferts, A.G. Roosenbrand, J.A.R. van Veen, J. Phys. Chem. B 102 (1998) 3445.

[40] W.-Y. Yu, L. Zhang, G.M. Mullen, E.J. Evans, G. Henkelman, C.B. Mullins, Phys. Chem. Chem. Phys. 17 (2015) 20588.

[41] H.Y. Kim, G. Henkelman, ACS Catal. 3 (2013) 2541.

[42] W.-Y. Yu, L. Zhang, G.M. Mullen, G. Henkelman, C.B. Mullins, J. Phys. Chem. C 119 (2015) 11754.

[43] M. Todorova, E. Lundgren, V. Blum, A. Mikkelsen, S. Gray, J. Gustafson, M. Borg, J. Rogal, K. Reuter, J.N. Andersen, M. Scheffler, Surf. Sci. 541 (2003) 101.

[44] I.-H. Svenum, J.A. Herron, M. Mavrikakis, H.J. Venvik, Catal. Today 193 (2012) 111.

[45] O.M. Løvvik, R.A. Olsen, J. Chem. Phys 118 (2003) 3268.

[46] S. González, K.M. Neyman, S. Shaikhutdinov, H.-J. Freund, F. Illas, J. Phys. Chem. C 111 (2007) 6852.

[47] O.M. Løvvik, S.M. Opalka, Surf. Sci. 602 (2008) 2840.

[48] J. Knudsen, J.N. Andersen, J. Schnadt, Surf. Sci. 646 (2016) 160.

[49] S. Urpelainen, C. Sathe, W. Grizolli, M. Agaker, A.R. Head, M. Andersson, S.-W. Huang, B.N. Jensen, E. Wallen, H. Tarawneh, R. Sankari, R. Nyholm, M. Lindberg, P. Sjoblom, N. Johansson, B.N. Reinecke, M.A. Arman, L.R. Merte, J. Knudsen, J. Schnadt, J.N. Andersen, F. Hennies, J. Synchrotron Rad. 24 (2017) 344.

[50] J. Schnadt, J. Knudsen, J.N. Andersen, H. Siegbahn, A. Pietzsch, F. Hennies, N. Johansson, N. Mårtensson, G. Öhrwall, S. Bahr, S. Mähl, O. Schaff, J. Synchrotron Rad. 19 (2012) 701.

[51] J.J. Yeh, I. Lindau, At. Data Nucl. Data Tables 32 (1985) 1.

[52] S. Doniach, M. Šunjić, J. Phys. C Solid State Phys. 3 (1970) 285.

[53] P. Kostelník, N. Seriani, G. Kresse, A. Mikkelsen, E. Lundgren, V. Blum, T. Šikola, P. Varga, M. Schmid, Surf. Sci. 601 (2007) 1574.

[54] W. Olovsson, C. Göransson, L. V. Pourovskii, B. Johansson, I.A. Abrikosov, Phys. Rev. B 72 (2005) 064203.

[55] Y. Jeon, Y.D. Chung, K.Y. Lim, C.N. Whang, J. Korean Phys. Soc. 37 (2000) 451.

[56] M. Van den Bossche, N.M. Martin, J. Gustafson, C. Hakanoglu, J.F. Weaver, E. Lundgren, H. Grönbeck, J. Chem. Phys. 141 (2014) 034706.

[57] J. Andersen, M. Qvarford, R. Nyholm, S. Sorensen, C. Wigren, Phys. Rev. Lett. 67 (1991) 2822.

[58] R. Toyoshima, N. Hiramatsu, M. Yoshida, K. Amemiya, K. Mase, B.S. Mun, H. Kondoh, J. Phys. Chem. C 120 (2016) 416.

[59] M. Smedh, A. Beutler, T. Ramsvik, R. Nyholm, M. Borg, J.N. Andersen, R. Duschek, M. Sock, F.P. Netzer, M.G. Ramsey, Surf. Sci. 491 (2001) 99.

[60] R. Toyoshima, M. Yoshida, Y. Monya, K. Suzuki, K. Amemiya, K. Mase, B.S. Mun, H. Kondoh, Phys. Chem. Chem. Phys. 16 (2014) 23564.

[61] D. Vogel, C. Spiel, Y. Suchorski, A. Trinchero, R. Schlögl, H. Grönbeck, G. Rupprechter, Angew. Chem. Int. Ed. Engl. 51 (2012) 10041.

FIGURE CAPTIONS

Figure 1: LEED images of the √5 surface oxide in UHV formed by oxidation in O_2, on (top) Pd_3Au (100) and (bottom) Pd (100) [35].

Figure 2: The Pd $3d_{5/2}$ core level of the √5 surface oxide under O_2 and CO at ratio 10:1 for (bottom) Pd(100) at 260°C [19], and (top) Pd_3Au(100) at 325°C.

Figure 3: The Pd $3d_{5/2}$ core level under O_2:CO=10:1 for Pd(100) (bottom) at 80°C [19], and Pd_3Au(100) (top) at ~25°C.

Figure 4: (a) O 1s temperature series for (bottom) heating Pd_3Au(100) from RT to 325°C and (top) cooling back down to 25°C in O_2 and CO at ratio 10:1, with corresponding QMS data for O_2, CO and CO_2. (b) O 1s core levels recorded at (bottom) RT, before starting the temperature increase, and (top) at 325°C. (c) The C1s core level spectrum acquired at 25°C just before starting the temperature ramp.

Figure 5: O 1s (left) and C 1s (right) core level spectra acquired for $Pd_3Au(100)$ at RT for O_2 to CO ratio 1:1.

Figure 6: O 1s (left) and Pd $3d_{5/2}$ (right) core level spectra acquired at ~ 300°C for $Pd_3Au(100)$ at O_2 to CO ratio 1:1.

Figure 7: CO_2 partial pressure during the temperature cycles as a function of temperature for (a) $Pd_3Au(100)$ under 10:1, and (b) Pd(100) (top) and $Pd_3Au(100)$ (bottom) under 1:1. Temperature increase and decrease is indicated with arrows.

FIGURES

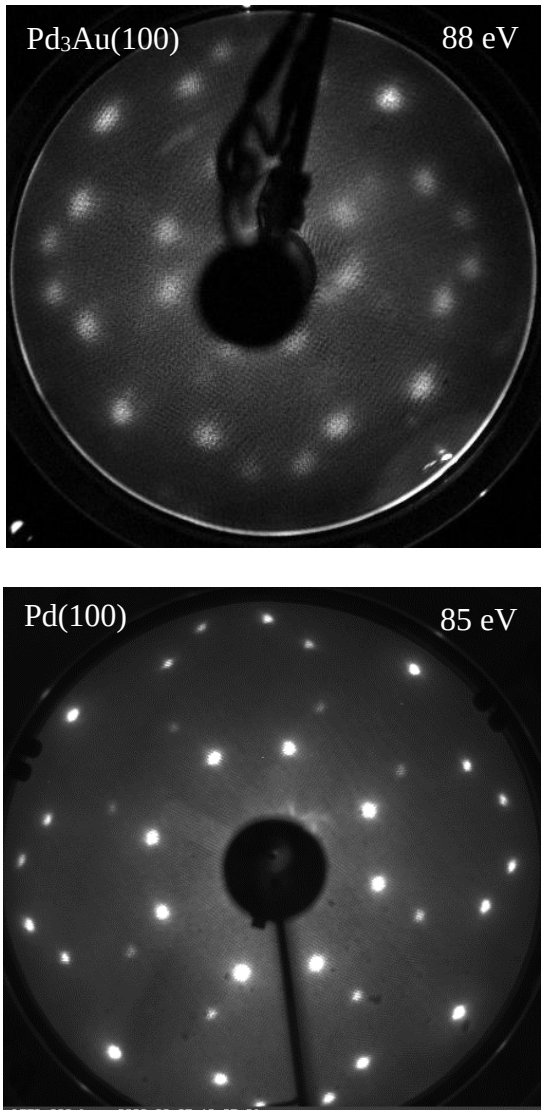

Figure 1: LEED images of the √5 surface oxide in UHV formed by oxidation in O_2, on (top) Pd_3Au (100), and (bottom) Pd (100), [35].

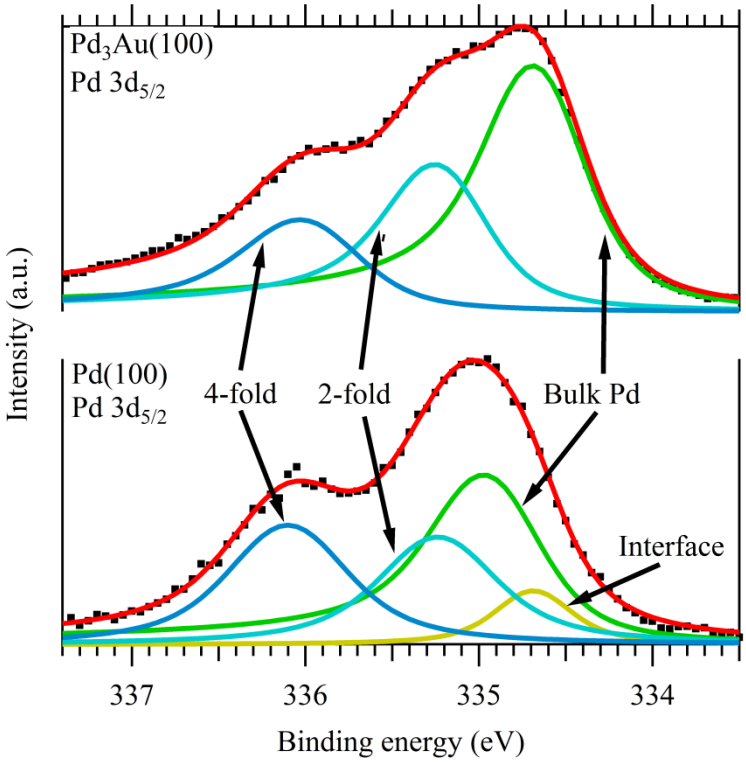

Figure 2: The Pd $3d_{5/2}$ core level of the √5 surface oxide under O_2 and CO at ratio 10:1 for (bottom) Pd(100) at 260°C [19], and (top) $Pd_3Au(100)$ at 325°C.

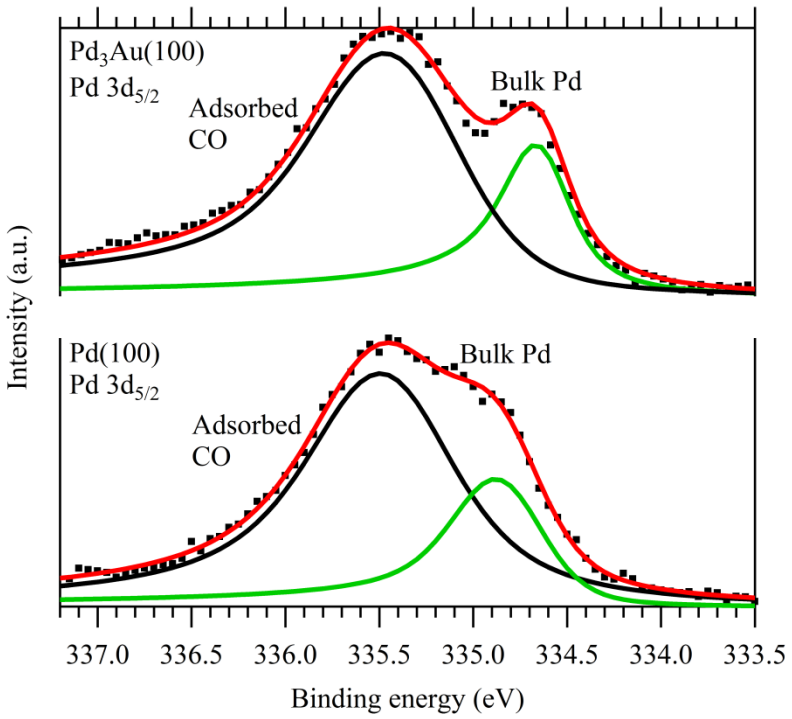

Figure 3: The Pd $3d_{5/2}$ core level under O_2:CO=10:1 for Pd(100) (bottom) at 80°C [19], and $Pd_3Au(100)$ (top) at ~25°C.

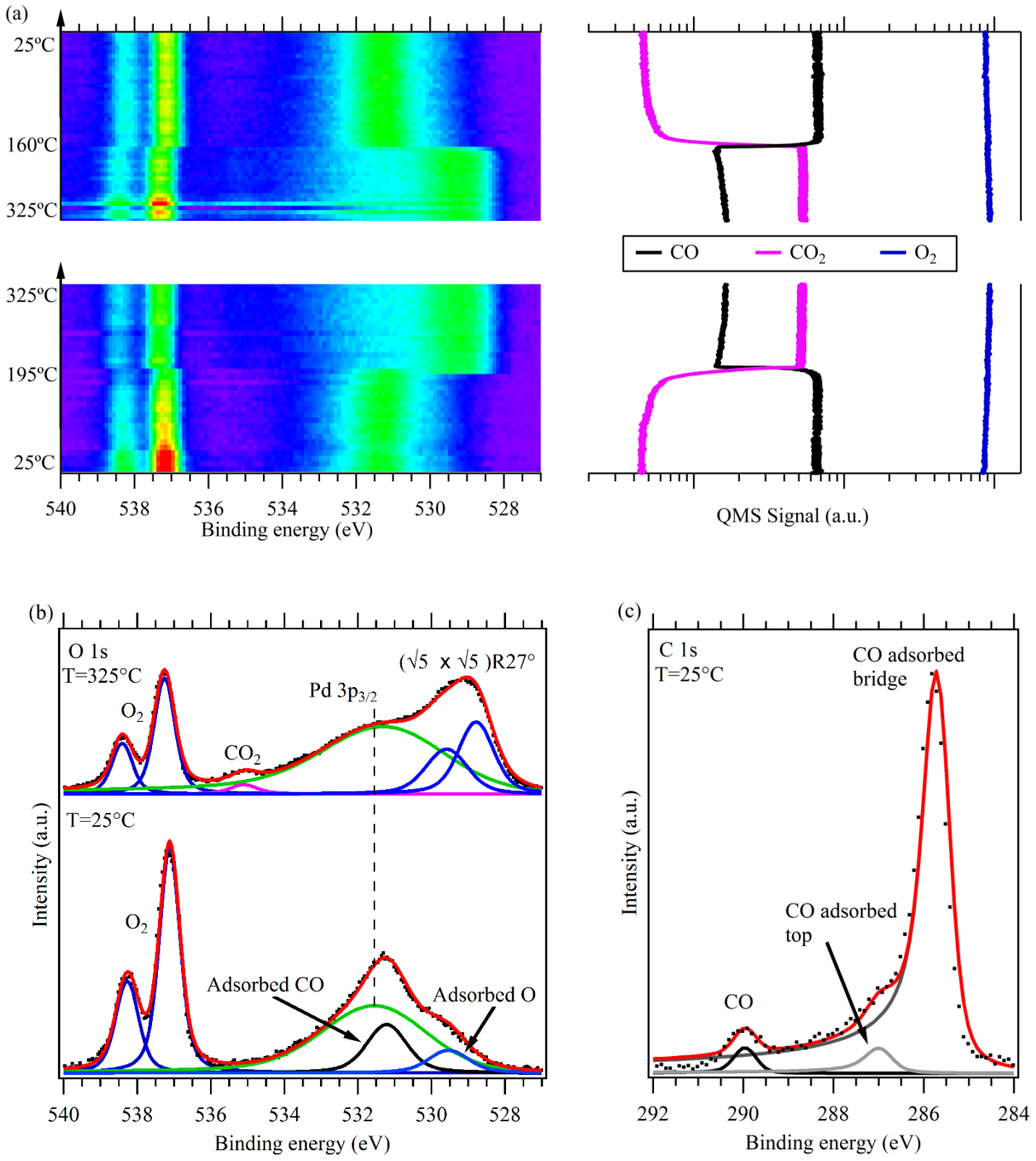

Figure 4: (a) O 1s temperature series for (bottom) heating $Pd_3Au(100)$ from RT to 325°C and (top) cooling back down to 25°C in O_2 and CO at ratio 10:1, with corresponding QMS data for O_2, CO and CO_2. (b) O 1s core levels recorded at (bottom) RT, before starting the temperature increase, and (top) at 325°C. (c) The C1s core level spectrum acquired at 25°C just before starting the temperature ramp.

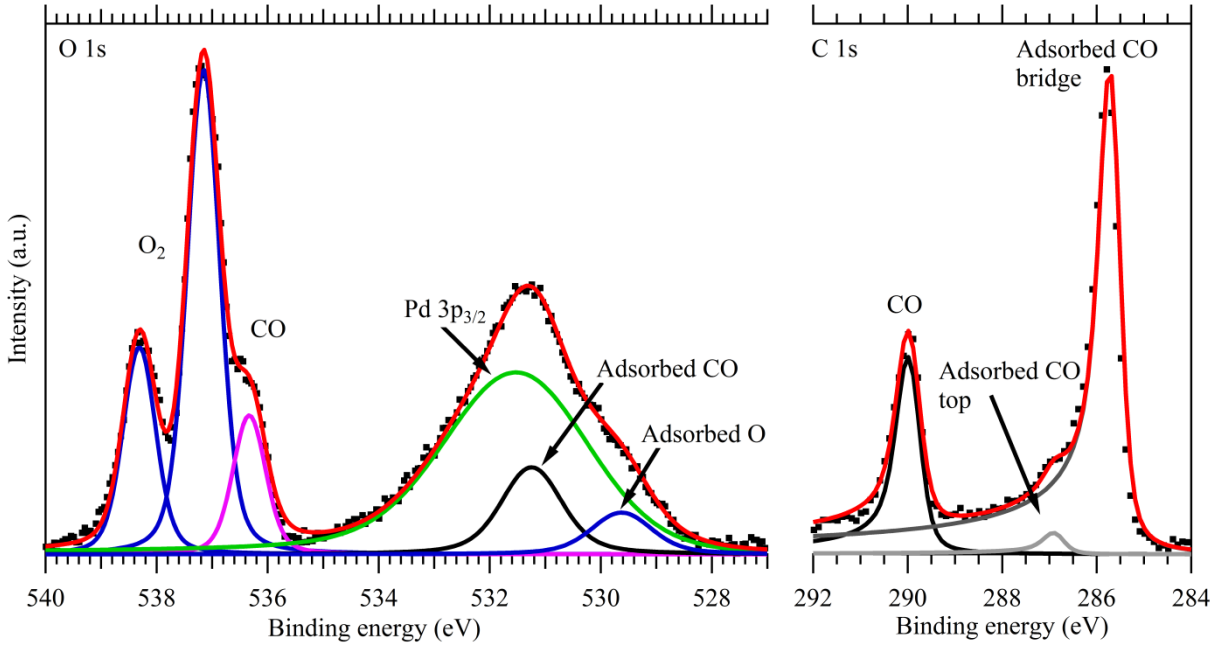

Figure 5: O 1s (left) and C 1s (right) core level spectra acquired for $Pd_3Au(100)$ at RT for O_2 to CO ratio 1:1.

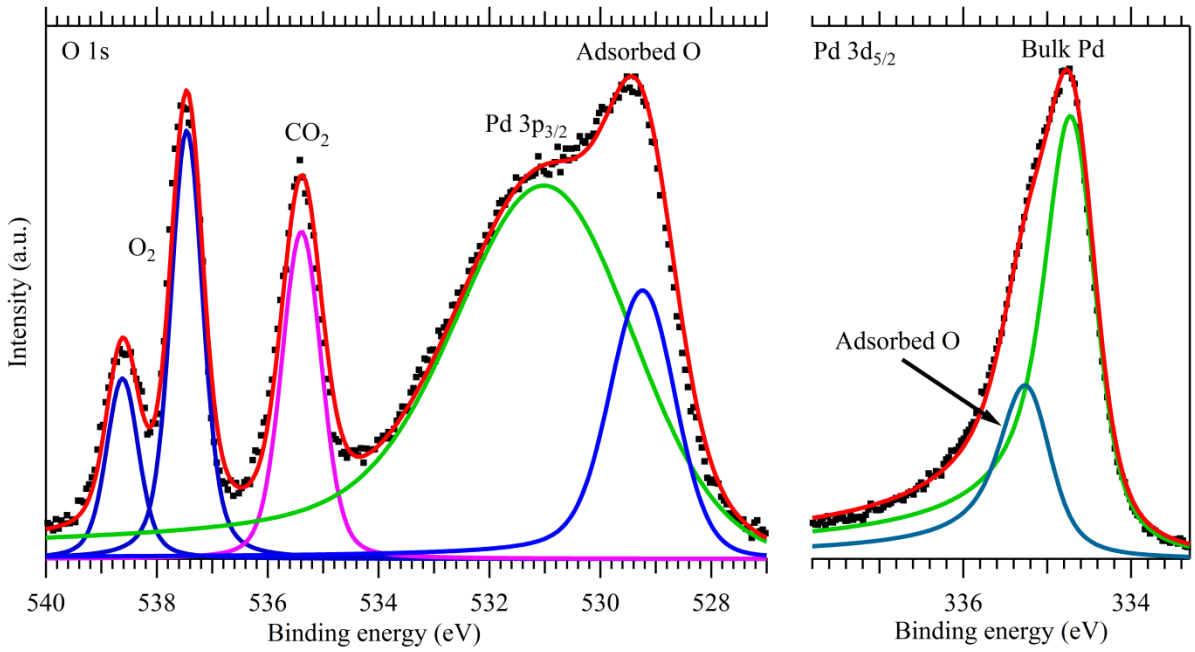

Figure 6: O 1s (left) and Pd $3d_{5/2}$ (right) core level spectra acquired at ~ 300°C for $Pd_3Au(100)$ at O_2 to CO ratio 1:1.

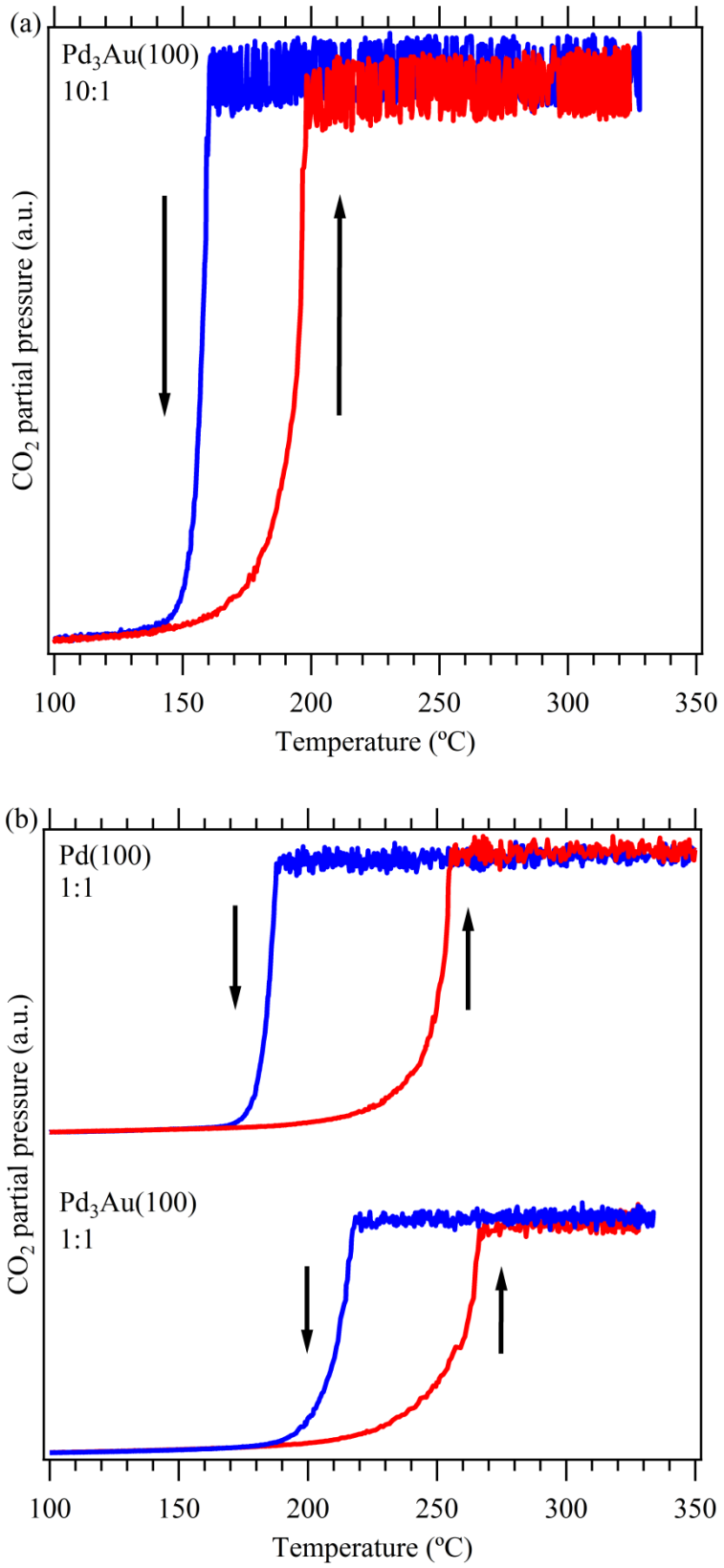

Figure 7: CO_2 partial pressure during the temperature cycles as a function of temperature for (a) $Pd_3Au(100)$ under 10:1, and (b) Pd(100) (top) and $Pd_3Au(100)$ (bottom) under 1:1. Temperature increase and decrease is indicated with arrows.